◆ Human Brain Mapping 29:1368–1378 (2008) ◆

Heritability of "Small-World" Networks in the Brain: A Graph Theoretical Analysis of Resting-State EEG Functional Connectivity

Dirk J. A. Smit,[1]* Cornelis J. Stam,[2] Danielle Posthuma,[1] Dorret I. Boomsma,[1] and Eco J. C. de Geus[1]

[1]*Department of Biological Psychology, VU University Amsterdam, Amsterdam, The Netherlands*
[2]*Department of Clinical Neurophysiology, VU University Medical Center*

Abstract: Recent studies have shown that resting-state functional networks as studied with fMRI, EEG, and MEG may be so-called small-world networks. We investigated to what extent the characteristic features of small-world networks are genetically determined. To represent functional connectivity between brain areas, we measured resting EEG in 574 twins and their siblings and calculated the synchronization likelihood between each pair of electrodes. We applied a threshold to obtain a binary graph from which we calculated the clustering coefficient *C* (describing local interconnectedness) and average path length *L* (describing global interconnectedness) for each individual. Modeling of MZ and DZ twin and sibling resemblance indicated that across various frequency bands 46–89% of the individual differences in *C* and 37–62% of the individual differences in *L* are heritable. It is asserted that *C*, *L*, and a small-world organization are viable markers of genetic differences in brain organization. *Hum Brain Mapp 29:1368–1378, 2008.*

Key words: EEG; resting state; synchronization likelihood; functional connectivity; heritability; twin study

INTRODUCTION

Brain connectivity is likely to have evolved under the constraints of optimized processing capacity while maintaining cost efficiency and resilience to loss of substrate [Achard and Bullmore, 2007; Bassett and Bullmore, 2006]. To describe such properties of neural networks, recent studies have applied graph theoretical methods on data obtained with MRI, fMRI, MEG, and EEG [e.g., Achard et al., 2006; Bassett and Bullmore; 2006; Micheloyannis et al., 2006a,b; Ponten et al., 2007; Stam, 2004]. Graph theory describes mathematical methods applied to representations of networks reduced to their essence: vertices (nodes) and edges (connections). In their ground-breaking article, Watts and Strogatz [1998] calculated two parameters to describe graphs derived from biological as well as nonbiological networks. The first describes the amount of local interconnectedness—or cliquishness—called clustering coefficient *C*. It takes a value between 0 and 1 indicating the proportion of neighboring vertices that are interconnected amongst each other. That is, if a neighbor is defined as a vertex that is one step removed, how many of the neighbors of one vertex are not only connected with

Contract grant sponsor: Human Frontiers of Science Program; Contract grant number: RG0154/1998-B; Contract grant sponsor: Netherlands Organization for Scientific Research; Contract grant numbers: NWO/SPI 56-464-14192, NWO/VIDI 452-05-318; Contract grant sponsor: Universitair Stimulerings Fonds; Contract grant number: USF 96/22.

*Correspondence to: D.J.A. Smit, Biologische Psychologie, van der Boechorststraat 1, 1081 BT Amsterdam, The Netherlands.
E-mail: dja.smit@psy.vu.nl

Received for publication 4 April 2007; Revised 16 July 2007; Accepted 17 July 2007

DOI: 10.1002/hbm.20468
Published online 6 December 2007 in Wiley InterScience (www.interscience.wiley.com).

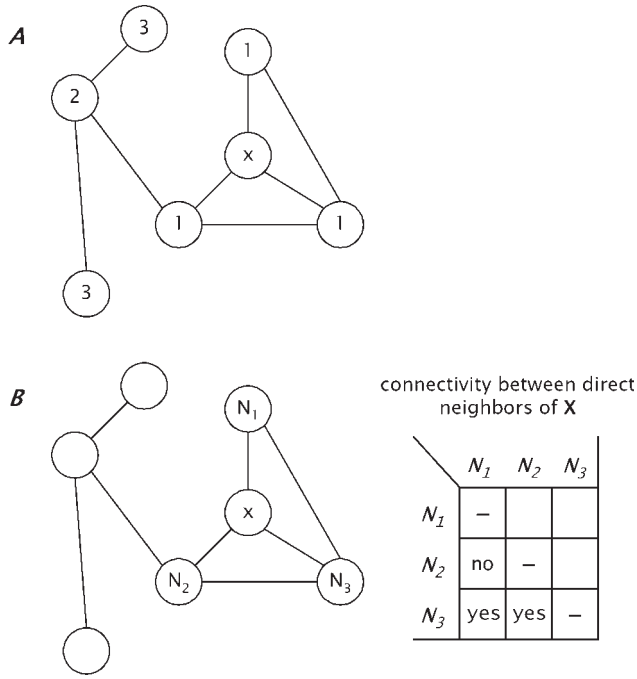

Figure 1.

(**A**) Average path length L for X is the average number of steps from node X to all other nodes: L_x = (1 + 1 + 1 + 2 + 3 + 3)/6 $ 1.8 (**B**). Clustering coefficient C for X describes proportional connectivity between the nodes neighboring node X: C_x = 2 out of 3 possible connections = 0.67.

that vertex, but also with each other. The second parameter describes global interconnectedness and is called the average path length *L*. It is a value simply indicating the average number of steps required to go from each vertex to all others taking the shortest route. Figure 1 shows a graphical explanation of the calculation of *C* and *L*.

Watts and Strogatz [1998] showed that *C* and *L* parameters represent non-trivial aspects of connection patterns along the dimension ranging from highly ordered graphs (lattices, regular networks) to fully randomized graphs. Ordered graphs are characterized by high *C* and long *L*. Random graphs have short *L* and low *C*. By starting from ordered graphs and randomly reconnecting single edges with a rewiring probability *P*, Watts and Strogatz showed that while the average path length *L* drops quickly, clustering coefficient *C* showed resilience against reconnection. Figure 2 shows the development of *C* and *L* against reconnection probability for a simulated 100-vertex graph with degree $K = 8$, where *K* represents the average number of edges per vertex. Ordered graphs, therefore, require only a few random long distance connections to drastically shorten the path length while maintaining a high clustering. Such efficient networks are designated "small-world," referring to the phenomenon that it takes surprisingly few steps to contact any two people in the world [Milgram, 1967] or to connect any actor to Kevin Bacon [wikipedia entry: six degree; of separation; Bassett and Bullmore, 2006]. Many types of existing networks have been shown to possess small-world features, including power grids, the world wide web, and as indicated, human societies.

In the realm of neural networks, a small-world topology has also been shown to exist in the neural network of *C. elegans* [Watts and Strogatz, 1998], in the brain anatomy in macaque and cat cortex [Hilgetag et al., 2000], and recently also in connectivity derived from cortical thickness measured in humans He et al., [in press]. Besides stationary anatomical connectivity, however, the brain also shows nonstationary functional connectivity between brain areas. Because of the high temporal resolution, EEG and MEG are particularly useful to study this kind of connectivity. Statistical interdependencies between EEG/MEG signals may serve as indices to these temporary connections between brain areas [or "effective connectivity"; Aertsen et al., 1989]. Although coherence is the most widely used linear measure of connectivity of EEG/MEG patterns, nonlinear measures of coupling may be more appropriate since brain activity is perhaps better modeled as an ensemble of coupled nonstationary, nonlinear dynamical subsystems [Friston, 2000; Pereda et al., 2005]. A relatively new measure that captures both the linear as well as nonlinear dependencies is synchronization likelihood (SL). With this measure, Stam and co-workers [Montez et al., 2006; Stam and van Dijk, 2002; Stam et al., 2003] have found that both linear and nonlinear synchronization are indeed present in normal background EEG/MEG. In addition, they suggested clinical usefulness of SL by showing that synchronization increased during and slightly before epileptic seizures; also, alpha, beta, and gamma band SL was decreased in Alzheimer's disease patients (for reviews see: Stam, 2005, 2006).

SL is based upon the concept of generalized synchronization as introduced by Rulkov et al. [1995]. Generalized

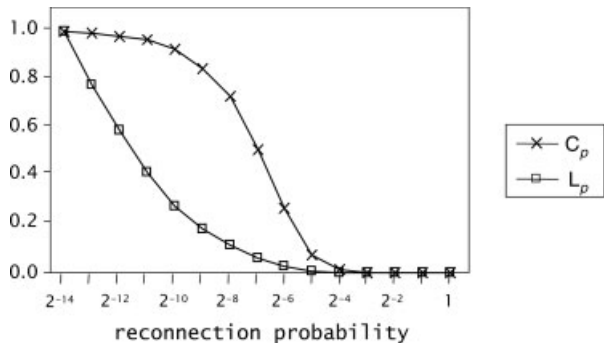

Figure 2.

Development of *C* and *L* as a function of the probability *p* of randomly rewiring of the edges of a 100 vertex ordered network with degree $K = 8$. Both C_p and L_p are scaled to a minimum of zero (a fully randomized network) and a maximum of one (a fully ordered network).

synchronization is said to exist between two dynamical systems X and Y if there exists a continuous one-to-one function F such that the state of one of the systems (the response system) can be mapped onto the state of the other system (the driver system): $Y = F(X)$ [Abarbanel et al., 1996; Kocarev and Parlitz, 1996; Rulkov et al., 1995]. Intuitively, this means that generalized synchronization exists between two systems X and Y if the following holds: if X is in the same state at two different times i and j, Y will also be in the same state at times i and j. By deriving the state of the system X from one EEG/MEG signal at a certain time point and the concurrent state of system Y, we can find evidence for connectivity between the brain areas whose activity is reflected in the signals. In sum, SL has the advantage over coherence as it will not show spurious connectivity between bandpass filtered white noise—in which case SL will assume the fixed, predefined value p_{ref}—, and is able to detect complex nonlinear coupling patterns. Detailed calculation procedures are presented in the Methods section.

The result of calculating SL between all possible pairs in a set of EEG/MEG signals can be interpreted as a general (linear and nonlinear) measure of connectivity strength in a functional network of brain areas. By application of a threshold, a sparsely connected graph can be created that is suitable for further graph theoretical analysis as proposed by Watts and Strogatz. Both C and L calculated from these graphs can be interpreted as measures of—local and global—efficiency [Barahona and Pecora, 2002; Lago-Fernandez et al., 2000; Latora and Marchiori, 2001; Masuda and Aihara, 2004]. Short L reduces the time or effort needed to connect two vertices, allowing efficient information exchange between, in this case, more distant brain regions. High C lowers the cost of building and maintaining localized networks and increases error tolerance in the case of loss of connectivity [Achard and Bullmore, 2007; Bassett and Bullmore, 2006]. Therefore, these parameters may reflect biologically important characteristics of the network.

The main focus of the current article is to determine whether individual differences in the network properties C and L, derived from resting state EEG functional connectivity, have a biological basis by establishing them as heritable traits. Heritability will be assessed by comparing C and L scores of MZ and DZ twins and their singleton siblings, who, having varying degrees of genetic relatedness, provide information on the amount of variation that can be attributed to genetic or environmental sources of variation [Boomsma et al., 2002a; Falconer and MacKay, 1996; Fisher, 1918].

Since it has been suggested that a small-world network architecture may be optimal for synchronizing neural activity between different brain regions, it seems plausible to hypothesize that individual differences in network properties C and L may be correlated with overall processing capacity or cognitive performance. Indeed, using EEG measured during a working memory task (the two-back task), higher educated subjects showed less of a small-world phenomenon than subjects with less education with almost the same behavioral performance [Micheloyannis et al., 2006a]. We will therefore investigate whether the same relation can be found between "small-worldness" and measures of general cognitive ability in the context of resting state EEG functional connectivity.

METHOD

Subjects

The sample for this study was derived from an ongoing twin-family study on cognition [Posthuma et al., 2001] in twins and family members from the Netherlands Twin Registry [Boomsma et al., 2002b]. Twins and siblings were invited for detailed psychophysiological study in the laboratory. The EEG sample consisted of 760 subjects from 309 families divided into two age cohorts based on the age of the twins: a younger cohort (M = 26.2 years, SD = 4.1) and a middle-aged cohort (M = 49.4 years, SD = 7.2). Participating families consisted of one to seven siblings (including twins). On average, 2.50 participants per family participated. Informed consent was obtained in writing for the EEG study. The study received approval from the appropriate ethical committees.

Intelligence Testing

IQ was measured with the Dutch adaptation of the WAISIII-R (WAIS-III, 1997). In accordance with the WAIS guidelines, the following four dimensions were calculated: verbal comprehension (the mean percentage correct of subtests information, similarities, and vocabulary), working memory (the mean percentage correct of subtests arithmetic and letter-number sequencing), perceptual organization (the mean percentage correct of subtests block design, matrix reasoning, and picture completion), and processing speed (the number of correct items per 60 s of subtest digit symbol substitution). The validity of these four dimensions was confirmed by a reanalysis of the WAIS manual data by Deary [2001]. From these dimensions the combined full scale IQ was determined.

EEG Recording

The experimental protocol for background EEG registration has been described in detail elsewhere [Posthuma et al., 2001; Smit et al., 2005], but a brief description will be repeated here. EEG was measured at rest. Half of registration sessions were during morning hours, and half were in the afternoon. Subjects were seated in a comfortable reclining chair in a dimly-lit, sound-attenuated, and electromagnetically-shielded room. They were instructed to close their eyes, relax, but stay awake and minimize eye and body movement. EEG was registered for 3 min with 17 Ag/AgCl electrodes mounted in an electrocap. Signal

registration was conducted using an AD amplifier developed by Twente Medical Systems (TMS; Enschede, The Netherlands) for 656 subjects (374 young, 282 middle-aged) and NeuroScan SynAmps 5083 amplifier for 104 subjects (24 young, 80 middle-aged). Signals were continuously represented online on a Nec multisync 17-in. computer screen using Poly 5.0 software or Neuroscan Acquire 4.2. Standard 10–20 positions were F7, F3, Fz, F4, F8, T7, C3, Cz, C4, T8, P7, P3, Pz, P4, P8, O1, and O2. The vertical electro-oculogram (EOG) was recorded bipolarly between two Ag/AgCl electrodes, affixed 1 cm below the right eye and 1-cm above the eyebrow of the right eye. The horizontal EOG was recorded bipolarly between two Ag/AgCl electrodes affixed 1 cm left from the left eye and 1 cm right from the right eye. An Ag/AgCl electrode placed on the forehead was used as a ground electrode. Impedances of all EEG electrodes were kept below 3 kΩ, and impedances of the EOG electrodes were kept below 10 kΩ. The EEG was amplified, digitized at 250 Hz and stored for off-line processing. Amplifier filter settings for TMS were a single order FIR bandpass filter with cut-off frequencies of 0.05 and 30.0 Hz. NeuroScan filter settings were a lowpass filter at 50.0 Hz.

EEG Data Processing

The signals were recalculated with averaged earlobes (A1 and A2) as reference. All EEG was automatically and visually checked for bad channels such as absence of signal, hum, clipping, persistent muscle tone artifacts, and external noise. Subjects without the full set of 17 leads were excluded. This procedure resulted in the exclusion of 186 subjects leaving 574 subjects. Next, the data were cut into 16 s epochs with 8 s overlap. For each subject, artifactual episodes were identified automatically using the EEGLAB [Delorme and Makeig, 2004] "reject by threshold" and "reject by spectra" option. Threshold settings for all leads was ±200 μV. The spectral analysis procedure identified deviant epochs by comparing each epoch's power spectrum to the spectrum averaged over all epochs. Epochs with more than 10-dB excess power within the frequency range below alpha (1.0–8.0 Hz) or above alpha (13.0–30.0 Hz) were marked artifactual. If less than four nonoverlapping epochs were available, the (quite strict) criterion of 10 dB was relaxed until exactly four were obtained. The average level of the dB criterium was 16.8 (SD 3.4). No subject reached a criterium level over 36 dB. Visual inspection revealed that this procedure successfully selected epochs without artifacts.

Each epoch was baseline corrected and filtered using theta (4.0–8.0 Hz), lower alpha (8.0–10.0 Hz), upper alpha (10.0–13.0), lower beta (13.0–18.0 Hz), and upper beta (18.0–25.0 Hz) bandpass filters. Frequencies above 25.0 Hz were disregarded as the discrepancies in hardware filter settings between TMS and Neuroscan registered subjects may lead to spurious results.

SL Calculation

The state of a driver system – here, an EEG signal – is operationalized with the embedded vector $X = \{x_i, x_i + 1^* l, x_i + 2^* l, \ldots, x_i + (m-1)^* l\}$ where l is the lag and m the embedding dimension. The elements of X are m samples taken from the signal spaced l apart. The vector is taken to represent the state of the system at time i. Within the same signal recurrences are sought at times j that reflect a similar state: a threshold distance ϵx is chosen such that a fixed proportion (p_{ref}) of comparisons are close enough to be considered in a similar state. Next, the same comparison is made for a different system Y at the same time points i and j and with the same value for p_{ref}. Now the SL S_i between X and Y at time i is defined as follows:

$$S_i = \frac{1}{N} \sum_j \theta(\varepsilon_y - |Y_i - Y_j|)\theta(\varepsilon_x - |X_i - X_j|)$$

where θ is the Heaviside step function returning 0 for all values <0 and 1 for values ≥ 0. N represents the number of recurrences in signal X, i.e.:

$$\sum_j \theta(\varepsilon_y - |X_i - X_j|)$$

Overall SL between X and Y is the average over all possible i. To withhold the system to compare X_i and X_j while they represent the same state, only values for j are considered that are at sufficient time distance. The value of this distance, $W1$, is the Theiler correction for autocorrelation [Theiler, 1986]. The value for $|i - j|$ is upper bound to create a window ($W1 < W2 < N$) to sharpen the time resolution of S_i. More details on SL calculation can be found in several other publications [Montez et al., 2006; Posthuma et al., 2005; Stam and van Dijk, 2002]. The parameter settings l, m, $W1$, and $W2$ were chosen based on the filter-frequency settings. This approach, as put forward in Montez et al. [2006], determines the lag l in sampling the embedded vector on the high frequency parameter of the filter, and the embedding dimension m on the ratio of the high and low frequency parameters. From these, windowing parameters $W1$ and $W2$ are chosen such that embedded vectors are not too close in time to avoid autocorrelation effects, while allowing enough estimations to be made. Table I shows the parameter settings for each frequency band. The remaining, free parameters $W2$ and p_{ref} were fixed at fixed values of $W1 + 400$ and 0.01. These values reflect similar choices from the previous literature [Ponten et al., 2007; Stam, 2006]. Using data from 51 randomly selected subjects revealed that a increasing the value of $W2$ from 430 to 830 did not change the results in the upper alpha band ($r = 0.99$). Increasing p_{ref} from 0.01 to 0.05 also yielded similar results ($r = 0.85$), adding to previous observations that variation of p_{ref} yields similar results [Stam and van Dijk, 2002].

TABLE I. Synchronization likelihood parameters per frequency band

Band	LF	HF	*L*	*m*	*W*1	*W*2
Theta	4	8	8	9	72	472
Lower alpha	8	10	6	6	36	436
Upper alpha	10	13	5	6	30	430
Lower beta	13	18	3	7	21	421
Upper beta	18	25	3	7	16	416

Note. LF, low frequency filter setting; HF, high frequency filter setting; *L*, Lag; *m*, embedding dimension; *W*1, minimum window distance; *W*2, maximum window distance. LF and HF are in Hz, all other parameters in number of samples.

C and *L* Calculation

SL was computed between each pair of electrodes resulting in a (17, 17) matrix where the values on the diagonal will be ignored. To correct for individual differences in overall SL this value was subtracted from the matrix of SL connectivity. Using this matrix to represent "edge strength," a binary graph was formed by applying a threshold θ such that the average number of edges per vertex was fixed at five different levels ($K \in \{3,4,5,6,7\}$). An actual example of a graph extracted from a single epoch is provided in Figure 3.

C and *L* were calculated as explained in the introduction and indicated in Figure 1 with the following extension. Standard *C* and *L* calculation requires that the graph is fully connected [Latora and Marchiori, 2001; Watts and Strogatz, 1998]. Many EEG epochs, however, resulted in graphs with at least one vertex unconnected. To accommodate for real world applications where unconnected nodes are unavoidable, we followed Newman's [2003] proposal to assign the value of $+\infty$ to the path length involving unconnected nodes and use the harmonic mean:

$$L = \frac{N}{\sum_{i=1}^{N} \frac{1}{L_i}}$$

For each graph we created 50 randomized graphs by randomly reconnecting edges, preserving the symmetry of the matrix. The average *C* and *L* values from these graphs were used to calculate standardized parameters [Humphries et al., 2006]:

$$\gamma = \frac{C}{C_{\text{ran}}}$$

and

$$\lambda = \frac{L}{L_{\text{ran}}}$$

The small world parameter was then calculated as $\sigma = \frac{\gamma}{\lambda}$. Since C_{ran} and L_{ran} are fixed numbers for graphs with the same degree *K*, there is no need to repeat the correlational analyses for γ and λ. Therefore, these analyses will be restricted to *C*, *L*, and σ.

Reliability and Twin Correlations

For all statistical modeling the freely available software package Mx version 1.65a was used [Neale et al., 2003].

A tetravariate repeated measures structural equation model as depicted in Figure 4 was used, which allows the estimation of the reliability of the measurement. Variance of the four occasions (epochs) is split into a correlated part *F* (the "true" scores) and an uncorrelated part *U* which we may assume represents measurement error. Reliability was then defined as the proportion of nonerror variance to the total:

$$R_{\text{epoch}} = \frac{f^2}{(f^2 + u^2)}$$

However, these single-epoch reliabilities should be corrected using the total number of epochs actually measured to represent reliability for the full 4×16 s duration using the following formula:

$$R_{\text{total}} = \frac{kR_{\text{epoch}}}{1 + (k-1)R_{\text{epoch}}}$$

where $k = 4$.

The correlation *r* in Figure 4 will be estimated to have the value r_{MZ} or r_{DZ}, depending on the nature of the relation between the two individuals. For twins and siblings members either an MZ or DZ/sibling correlation will be

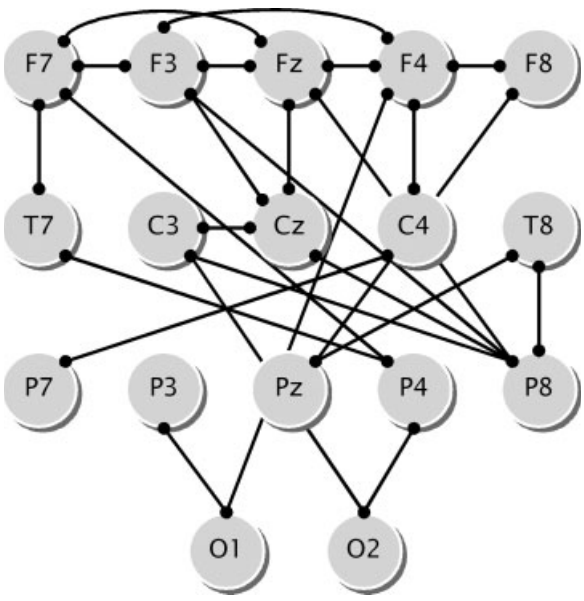

Figure 3.
An example of a graph derived from the Synchronization Likelihood matrix for a single epoch.

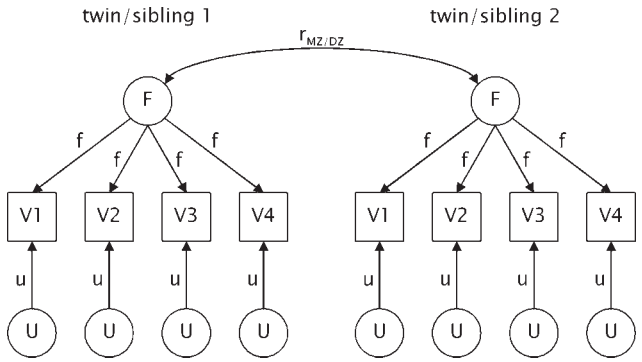

Figure 4.

Path model describing the relation between any pair of siblings. *V1*, *V2*, *V3*, and *V4* represent the observed variables *C*, *L*, or σ from the four epochs. Factors U are uncorrelated and represent unreliable factors such as measurement error. F is "true" factor scores representing the remaining variance. Depending on the relation between the two subjects, an r_{MZ} (MZ twins), r_{DZ} (DZ twins and siblings) is modeled.

estimated. Note that the resulting twin correlations represent the relation between "true" factors *F*, and are thus corrected for measurement error.

Means were modeled with cohort and sex and the cohort by sex interaction as covariates. Variances were tested for heteroscedasticity between the sexes and the cohorts. When significant, heteroscedasticity were modeled by using a scalar model. These models use a scalar close to 1.0 to equalize the variances in one group (e.g., males) to the other (e.g., females). Significant differences in error variances were modeled similarly.

Genetic analyses

Resemblance (covariance) in psychophysiological traits between twins and siblings derive from genetic relatedness or shared environmental influences [Boomsma et al., 2002a; Falconer and Mackay, 1996]. If the correlation between DZ twins or siblings, who share on average 50% of their genetic make-up, is half the correlation between MZ twins, who are genetically identical, this is seen as evidence for additive genetic influences (A). If the correlation between DZ twins or siblings is less than half the correlation between MZ twins this is seen as evidence for dominant (nonadditive) genetic influences (D). If the correlations between MZ and DZ twins/siblings are comparable and nonzero this is evidence for shared environmental influences (S). If the correlation between MZ twins is not unity this is evidence for environmental effects unique to each individual (E). By comparing MZ and DZ/sibling correlations, using structural equation modeling as implemented in, for example, Mx [Neale et al., 2006], we can obtain maximum likelihood estimates of the relative contributions of each of these factors to the total trait variance. Heritability is defined as the proportional contribution of genetic effects (A + D) to the total variance (A + S + D + E). In a twin-sibling design, however, no information is available to estimate the effects of both S and D simultaneously. The relative size of the DZ/sibling to the MZ correlation guides which is selected. If the DZ/sibling correlation is less than half the MZ correlation, then A + D + E are modeled. If it is more than half the MZ correlation, A + S + E are modeled. For more information on genetic modeling we refer to Boomsma et al. [2002a] and Posthuma et al. [2003].

WAIS Correlations

Correlations were calculated between *C*, *L*, and σ and scores on the four subscales verbal comprehension, working memory, perceptual organization, and perceptual speed. Since dependencies exist between family members, statistical inference from straightforward correlations between traits would be incorrect. We therefore modeled the correlations while allowing for within family correlations (i.e., MZ and DZ/sibling correlations, and cross-twin-cross-trait correlations). As with all other modeling, the correlations were modeled on the "true," nonerror variance of *C*, *L*, and σ.

RESULTS

Unconnected Vertices

It may have been possible that one lead resulted in an unconnected vertex in most subjects, suggesting that this lead should be removed from the analysis. Although T7 and T8 showed quite a high proportion of epochs which resulted in unconnected vertices, still in about 60% of the epochs they were connected. Therefore, we decide not to exclude these leads.

Descriptives

Table II shows the descriptives for parameters *C* and *L*, and the derived variables γ, λ and σ Since the distributions for λ were in many cases right skewed, median values are shown to define central tendency. Overall, these parameters are consistent with a small-world organization of the functional network, since λ is relatively close to unity, whereas γ is larger than that (see Table II). For all explored levels of *K*, gamma was clearly and significantly larger than unity. However, increasing *K* resulted in reduced levels of gamma (as can be expected). The median value for the variable λ is only slightly larger than unity for higher degrees of K ($K \geq 5$). Lower values of *K* showed clearer deviation from unity with values above 1.1 in all frequency bands.

Levels of *K*

To explore the nature of the dependency of the graph variables *C* and *L* on degree *K* we calculated the correlation of the

TABLE II. Medians and interquartile ranges for graph theoretical parameters of functional connectivity

	C		L		γ		λ		σ	
Band	Me	Quart. range	Me	Quart. range	Me	Quart. range	Me	Quart. range	Me	Quart. range
$K = 3$										
Theta	0.34	0.31–0.38	2.67	2.49–2.92	2.23	2.00–2.45	1.20	1.12–1.31	1.80	1.66–1.97
Lower alpha	0.37	0.33–0.40	2.90	2.62–3.17	2.33	2.12–2.55	1.31	1.19–1.44	1.74	1.60–1.88
Upper alpha	0.36	0.33–0.39	2.80	2.57–3.09	2.30	2.08–2.50	1.27	1.17–1.40	1.76	1.62–1.92
Lower beta	0.35	0.32–0.38	2.67	2.51–2.87	2.20	2.01–2.39	1.21	1.14–1.30	1.76	1.63–1.93
Upper beta	0.35	0.32–0.38	2.78	2.58–3.07	2.23	2.04–2.44	1.26	1.17–1.39	1.72	1.57–1.86
$K = 4$										
Theta	0.41	0.38–0.44	2.06	1.98–2.17	1.78	1.67–1.91	1.10	1.06–1.16	1.59	1.49–1.70
Lower alpha	0.44	0.41–0.47	2.27	2.09–2.50	1.91	1.77–2.05	1.21	1.12–1.34	1.54	1.43–1.66
Upper alpha	0.44	0.41–0.47	2.19	2.07–2.40	1.89	1.75–2.03	1.17	1.11–1.28	1.55	1.45–1.67
Lower beta	0.43	0.40–0.46	2.13	2.03–2.27	1.85	1.73–1.98	1.14	1.08–1.22	1.59	1.49–1.69
Upper beta	0.44	0.41–0.47	2.24	2.07–2.44	1.89	1.74–2.01	1.20	1.11–1.31	1.54	1.43–1.65
$K = 5$										
Theta	0.46	0.44–0.50	1.76	1.72–1.81	1.52	1.44–1.62	1.04	1.02–1.08	1.44	1.36–1.52
Lower alpha	0.51	0.48–0.54	1.89	1.80–2.05	1.67	1.57–1.76	1.13	1.07–1.22	1.44	1.37–1.53
Upper alpha	0.51	0.48–0.54	1.84	1.77–1.98	1.66	1.56–1.77	1.10	1.06–1.18	1.47	1.39–1.55
Lower beta	0.50	0.47–0.53	1.82	1.74–1.92	1.63	1.53–1.74	1.08	1.04–1.14	1.48	1.40–1.55
Upper beta	0.51	0.47–0.54	1.88	1.79–2.02	1.65	1.54–1.75	1.12	1.06–1.20	1.44	1.36–1.51
$K = 6$										
Theta	0.50	0.48–0.53	1.60	1.59–1.63	1.37	1.30–1.45	1.02	1.01–1.04	1.33	1.28–1.39
Lower alpha	0.57	0.54–0.59	1.69	1.63–1.78	1.53	1.45–1.61	1.08	1.04–1.14	1.39	1.33–1.46
Upper alpha	0.56	0.54–0.59	1.66	1.62–1.74	1.52	1.44–1.60	1.06	1.03–1.11	1.41	1.34–1.47
Lower beta	0.55	0.53–0.59	1.64	1.60–1.73	1.50	1.42–1.59	1.05	1.02–1.10	1.40	1.34–1.47
Upper beta	0.56	0.53–0.60	1.71	1.62–1.81	1.52	1.43–1.61	1.09	1.03–1.16	1.38	1.31–1.44
$K = 7$										
Theta	0.55	0.53–0.57	1.49	1.49–1.50	1.25	1.20–1.31	1.01	1.00–1.01	1.24	1.20–1.29
Lower alpha	0.62	0.58–0.65	1.54	1.50–1.60	1.41	1.34–1.47	1.04	1.01–1.08	1.33	1.28–1.38
Upper alpha	0.61	0.59–0.65	1.52	1.50–1.57	1.40	1.34–1.47	1.03	1.01–1.06	1.34	1.29–1.40
Lower beta	0.60	0.57–0.65	1.51	1.49–1.59	1.38	1.30–1.47	1.02	1.01–1.07	1.32	1.26–1.38
Upper beta	0.62	0.58–0.66	1.56	1.50–1.65	1.41	1.33–1.50	1.05	1.01–1.11	1.32	1.26–1.38

graph descriptors C and L between all levels of K. Next, we averaged the correlations (using the Fisher transform) to obtain marginals representing the strength of correlation between a each level of K with all other levels. Table III shows the average correlations for C and L in all frequency bands. For C, the correlations are somewhat smaller than those for L, but still moderate to high (ca. 5 for $K = 3$ but 0.6 to 0.7 for other levels). For L, correlations between levels are high. Degree $K = 3$ seems to correlate the worst with all other levels, whereas $K = 5$ seems to correlate best for both C ($r > 0.67$) and L ($r > 0.83$) in all frequency bands.

Overall, $K = 5$ seems to be the best representation of most of the variation shared between all levels of K. In addition, C and L at degree $K = 5$ seems to show small world network properties as mentioned in the previous paragraph. To reduce the amount of further testing, we chose to restrict the genetic and phenotypic analyses to graphs with degree $K = 5$.

Effects on Means and Variances

Sex differences in L were found in the lower frequency bands such that males show shorter L (theta: $\beta_{sex} = 0.026$, $\chi^2(1) = 7.70$, $P = 0.006$; lower alpha: $\beta_{sex} = 0.045$, $\chi^2(1) = 8.30$, $P = 0.004$). No other significant mean sex differences were found. The middle-aged cohort showed significantly lower C for the theta band ($\beta_{coh} = -0.011$, $\chi^2(1) = 8.53$, $P = 0.003$), but higher C for upper alpha ($\beta_{coh} = 0.011$, $\chi^2(1) = 8.52$, $P = 0.004$). Middle-aged adults showed longer L in both these bands (theta: $\beta_{coh} = 0.028$, $\chi^2(1) = 8.53$, $P = 0.003$; upper alpha: $\beta_{coh} = 0.077$, $\chi^2(1) = 24.4$, $P = 1 \times 10^{-6}$). In the theta band this resulted in a significantly lower value of the small-world variable sigma for the middle-aged ($\beta_{coh} = -0.029$, $\chi^2(1) = 8.14$, $P = 0.004$).

Variances differed between the sexes only for L in the theta band ($\chi^2(1) = 17.5$, $P = 3 \times 10^{-5}$). In males "true" variance was larger than in females. Large differences in true variance were also found between the cohorts (theta: $\chi^2(1) = 57.0$, $P = 4 \times 10^{-14}$; upper alpha: $\chi^2(1) = 17.8$, $P = 2 \times 10^{-5}$), such that the older cohort had larger variances in L than the younger cohort.

Reliabilities

Reliabilities were calculated using the repeated measures model and corrected to represent reliability of the full measurement as specified in the methods. Table IV shows that the reliabilities were, in general, moderate for C and σ. This indicates that measurement error covered a substantial proportion of the variance of C (~50%) and slightly more of σ (~50% to 65%). This proportion was larger for the lower frequency bands. The proportion mea-

TABLE III. The correlations between scores on each level of *K* and scores on all other levels, averaged using Fisher transform, variables *C* and *L*

	K				
	3 with 4,5,6, and 7	4 with 3,5,6, and 7	5 with 3,4,6, and 7	6 with 3,4,5, and 7	7 with 3,4,5, and 6
C					
Theta	0.52	0.59	0.68	0.65	0.63
Lower alpha	0.54	0.64	0.69	0.69	0.63
Upper alpha	0.50	0.60	0.67	0.67	0.63
Lower beta	0.45	0.59	0.69	0.67	0.65
Upper beta	0.52	0.65	0.72	0.71	0.66
L					
Theta	0.67	0.79	0.83	0.81	0.74
Lower alpha	0.78	0.85	0.88	0.87	0.82
Upper alpha	0.79	0.86	0.89	0.88	0.80
Lower beta	0.79	0.87	0.89	0.89	0.84
Upper beta	0.75	0.85	0.89	0.88	0.82

surement error was markedly less for L than for C and σ. Note that in some cases heterogeneity of variance and/or error variance were found (as aforementioned). Since these differences resulted in different reliabilities for sex or age cohort groups, Fisher-z transformed averages (transformed back) are shown in the table in those cases.

Genetic Analysis

Genetic models included aforementioned significant effects on the means and variances. Men and women and the older and younger cohorts did not differ in MZ and DZ/sibling correlations. The resulting twin correlations—collapsed across cohort and sex—are shown in Table V along with 95% confidence intervals.

Although the twin correlations suggested effects of shared environment for theta band L, this effect was not significant. Significant dominant genetic effects were found for L for the theta and upper alpha bands ($\chi^2(1) = 8.9$, $P = 0.0003$, and $\chi^2(1) = 10.1$, $P = 0.002$, respectively). For these variables broad heritabilities were estimated, that is, including both dominant and additive genetic variance, and a two degree of freedom test determining the significance of both the effects of A and D simultaneously. All heritabilities are shown in Table VI. Highly significant heritability could be established for L in all frequency bands (lowest significance for theta: $\chi^2(2) = 18.5$, $P = 1 \times 10^{-4}$). Significant heritability for C was found in the theta and beta frequency bands (theta: $\chi^2(1) = 8.5$, $P = 0.004$; lower beta: $\chi^2(1) = 14.9$, $P = 1 \times 10^{-4}$; upper beta: $\chi^2(1) = 17.6$, $P = 3 \times 10^{-5}$). Heritability estimates for σ on the other.

DISCUSSION

The results for parameters $\gamma(L/L\text{ran})$, $\lambda(C/C\text{ran})$, and $\sigma = \frac{\gamma}{\lambda}$ derived from functional connectivity graphs with degree $K = 5$ are comparable to those reported in the existing literature and summarized in Table VII. Functional connectivity graphs derived from fMRI, MEG, and EEG have shown values for λ in the range of 1.0–1.5, but are typically around 1.1 which is highly comparable to our 1.04–1.13. Values for γ from the same studies ranged from 1.58 to 3.77. The values reported here (1.52 to 1.67) are at

TABLE IV. Reliable, nonerror variance as a proportion of total variance for graphs with degree *K* = 5

	C	*L*	σ
Theta	0.48	0.71	0.33
Alpha low	0.53	0.77	0.41
Alpha high	0.52	0.77	0.41
Beta low	0.52	0.86	0.41
Beta high	0.62	0.87	0.47

Note. For some variable ICCs differed between cohorts and/or sexes due to heterogeneity of variance or heterogeneity of error variance. Average values are shown. Reliabilities are based on the correlations between all epochs, then corrected to represent reliability of the total of four epochs. C = clustering coefficient, L = average path length, σ = small world variable γ/λ.

TABLE V. Twin correlations for *C*, *L*, and σ for graphs with degree *K* = 5

	C		*L*		σ	
	MZ	DZ	MZ	DZ	MZ	DZ
Theta	0.60	0.18	0.93***	0.12	0.74	−0.01*
Lower alpha	0.51	0.10	0.55***	0.14	0.52	0.28
Upper alpha	0.49	0.10	0.81***	−0.01*	0.26	−0.22
Lower beta	0.66*	0.26	0.49***	0.34	0.58	−0.03
Upper beta	0.53*	0.28	0.70***	0.35	0.47	0.14

Note. All correlations were estimated using Mx after removal of age and sex on the means, and significant cohort and sex effects on variance terms by use of a scalar model. DZ correlations include all fraternal (non-identical) siblings pairs, including opposite sex pairs. *C*, Clustering coefficient, *L*, Path length, σ, small world index γ/λ* = $P < 0.01$; **$P < 0.001$; ***$P < 0.0001$.

TABLE VI. Heritabilities for C, L, and σ

	C		*L*		σ
Theta	0.50	*	0.89	*	0.37
Lower alpha	0.37		0.46	***	0.51
Upper alpha	0.39		0.78	***	0.00
Lower beta	0.62	**	0.53	***	0.27
Upper beta	0.54	***	0.70	***	0.39

Note. Heritability was modeled using additive genetic and unique environmental effects, except for: Dominant genetic effects were significant for theta *L* and upper alpha *L*. For these, heritability (h^2) includes both additive and non-additive (dominant) genetic effects.
*$P < 0.01$, **$P < 0.001$, ***$P < 0.0001$. *C*, clustering coefficient; *L*, average path length; σ, small world index: γ/λ.

the lower end of this previously reported range, although this seems consistent with the results from the other EEG studies. Small world parameter σin the literature ranged from 1.56 to 2.79. Here, too, our results were at the low end of the dimension with 1.44–1.48. However, the small world requirement defined as $\lambda = 1.0$ while $\gamma \gg 1.0$ seems to be met.

Modeling of MZ and DZ twin and sibling resemblance indicated that across various frequency bands 46–89% of the individual differences in *C* and 37–62% of the individual differences in *L* are heritable. Overall, these results suggest that there are consistent individual differences in functional connectivity patterns that have a firm biological basis. Graph theoretical analysis of background EEG connectivity reveals systematic individual differences in average path length *L* and clustering coefficient *C*, which makes them viable biomarkers for individual differences in brain functioning. However, unreliable variance constitutes a large part of the total variance of mainly *C*. If the unreliable variance can indeed be attributed to measurement error, that this finding indicates the importance of measuring many epochs of sufficient length to obtain reliable estimates of individual scores. In the present study, measuring four epochs did not yield sufficient power to establish significance of the heritability estimates for the overall network efficiency as measured with σ.

Since it has been argued that *C* and *L* are parameters that describe network efficiency, it was reasonable to hypothesize that efficient connectivity patterns would be related to cognitive performance measures. However, we found that WAIS was not significantly related to either *C*, *L*, or small-world parameter σ. Although individual differences in *C* and *L* may simply not reflect those in cognitive performance, the absence of significant correlation may also have been the result of suboptimal measurement evidenced by the substantial amount of error variance. In addition, the application of a threshold to the SL matrix resulted in the loss of possibly valuable information regarding the connectivity strength between brain areas. To make use of this source of information, alternative approaches for investigating network efficiency to the one presently used have been proposed. For example, Latora and Marchiari [2001] proposed a method to describe local and global efficiency computed from what have been called weighted graphs. It stands to reason that such an approach could result in better estimations of overall network efficiency, and hence, better estimates of phenotypic correlations. Ultimately, though, this remains an empirical question. Another possible source of bias is that volume conduction in the EEG signals could have falsely increased

TABLE VII. Graph theoretical parameters from psychophysiological studies of functional connectivity

Study	Sample	Measurement	Condition	λ	γ	σ
Current study	Healthy subjects	EEG theta, low alpha, high alpha, low beta, high beta, *K*=5	Resting state	1.09	1.63	1.45
Achard et al., 2006	Healthy subjects	fMRI .0007-.45 Hz[a]	Resting state	1.14	2.18	1.94
Bartolomei et al., 2006	Healthy subjects	MEG theta, beta, gamma	Resting state	~1.5	~4.0	2.67
Bassett et al., 2006	Healthy subjects	MEG 1.1-75 Hz[a]	Resting state			1.92
			Finger tapping			1.86
Eguiluz et al., 2005[b]	Healthy subjects	FMRI	Music listening and finger tapping	1.0–2.9	168–325	
Micheloyannis et al., 2006	Schizophrenia	EEG theta, alpha, beta, gamma	WM task	1.15	1.64	1.43
	Healthy subjects			1.15	1.80	1.56
Ponten et al., 2007	Epileptic patients	Depth electrode EEG, 1 to 48 Hz synchronization	Interictal periods	1.1	1.72	1.56
Salvador et al., 2005	Healthy subjects	FMRI	Resting state	1.09	2.08	1.91
Stam et al., 2004	Healthy subjects	MEG theta, gamma[c]	Resting state	1.41	3.76	2.68
Stam et al., 2006	Alzheimer's	MEG beta	Resting state	1.12	1.6	1.43
	healthy subjects			1.07	1.58	1.48

Results as summarized by the respective authors, except:
[a] No averages reported by the authors, values averaged across frequencies are shown.
[b] The degree K was much smaller than ln(N), which may have caused the anomalous results (see Bassett & Bullmore, 2006).
[c] Stam, 2004 did not find small-world organization in the alpha and beta frequency bands (omitted here).

connectivity strengths of nearby electrodes. Therefore, recently proposed measures that take volume conduction into account, such as the phase lag index [Stam et al., in press] could possibly alleviate this problem. Lastly, using a single degree K for all individuals may have disregarded "true" differences between subjects, that is, some subjects may simply have a more sparsely connected functional network. Again, this too remains an empirical question.

In conclusion, graph theory is a useful tool for describing functional connectivity of the brain. The pattern of twin correlations for C, L, and σ establish them as viable markers of genetic differences in brain organization.

REFERENCES

Abarbanel HD, Rulkov NF, Sushchik MM (1996): Generalized synchronization of chaos: The auxiliary system approach. Phys Rev E 53:4528–4535.

Achard S, Bullmore E (2007): Efficiency and cost of economical brain functional networks. PLoS Comput Biol 3:e17.

Achard S, Salvador R, Whitcher B, Suckling J, Bullmore E (2006): A resilient, low-frequency, small-world human brain functional network with highly connected association cortical hubs. J Neurosci 26:63–72.

Aertsen AM, Gerstein GL, Habib MK, Palm G (1989): Dynamics of neuronal firing correlation: Modulation of "effective connectivity." J Neurophysiol 61:900–917.

Barahona M, Pecora LM (2002): Synchronization in small-world systems. Phys Rev Lett 89:054101.

Bartolomei F, Bosma I, Klein M, Baayen JC, Reijneveld JC, Postma TJ, Heimans JJ, van Dijk BW, de Munck JC, de Jongh A, Cover KS, Stam CJ (2006): How do brain tumors alter functional connectivity? A magnetoencephalography study. Ann Neurol 59:128–138.

Bassett DS, Bullmore E (2006): Small-world brain networks. Neuroscientist 12:512–523.

Bassett DS, Meyer-Lindenberg A, Achard S, Duke T, Bullmore E (2006): Adaptive reconfiguration of fractal small-world human brain functional networks. Proc Natl Acad Sci USA 103:19518–19523.

Boomsma D, Busjahn A, Peltonen L (2002a): Classical twin studies and beyond. Nat Rev Genet 3:872–882.

Boomsma DI, Vink JM, van Beijsterveldt TC, de Geus EJ, Beem AL, Mulder EJ, Derks EM, Riese H, Willemsen GA, Bartels M, et al. (2002b): Netherlands Twin Register: A focus on longitudinal research. Twin Res 5:401–406.

Deary IJ (2001): Human intelligence differences: A recent history. Trends Cogn Sci 5:127–130.

Delorme A, Makeig S (2004): EEGLAB: An open source toolbox for analysis of single-trial EEG dynamics including independent component analysis. J Neurosci Methods 134:9–21.

Eguiluz VM, Chialvo DR, Cecchi GA, Baliki M, Apkarian AV (2005): Scale-free brain functional networks. Phys Rev Lett 94:018102.

Falconer DS, MacKay TF (1996): Quantatative Genetics. Harlow: Prentice Hall.

Fisher RA (1918): The correlation between relatives on the supposition of mendelian inheritance. Philos Trans R Soc Edinb 52: 399–433.

Friston KJ (2000): The labile brain. I. Neuronal transients and nonlinear coupling. Philos Trans R Soc Lond B Biol Sci 355:215–236.

He Y, Chen ZJ, Evans AC. Small-world anatomical networks in the human brain revealed by cortical thickness from MRI. Cereb Cortex. (epub ahead of print).

Hilgetag CC, O'Neill MA, Young MP (2000): Hierarchical organization of macaque and cat cortical sensory systems explored with a novel network processor. Philos Trans R Soc Lond B Biol Sci 355:71–89.

Humphries MD, Gurney K, Prescott TJ (2006): The brainstem reticular formation is a small-world, not scale-free, network. Proc Biol Sci 273:503–511.

Kocarev L, Parlitz U (1996): Generalized synchronization, predictability, and equivalence of unidirectionally coupled dynamical systems. Phys Rev Lett 76:1816–1819.

Lago-Fernandez LF, Huerta R, Corbacho F, Siguenza JA (2000): Fast response and temporal coherent oscillations in small-world networks. Phys Rev Lett 84:2758–2761.

Latora V, Marchiori M (2001): Efficient behavior of small-world networks. Phys Rev Lett 87:198701.

Masuda N, Aihara K (2004): Global and local synchrony of coupled neurons in small-world networks. Biol Cybern 90: 302–309.

Micheloyannis S, Pachou E, Stam CJ, Vourkas M, Erimaki S, Tsirka V (2006a): Using graph theoretical analysis of multi channel EEG to evaluate the neural efficiency hypothesis. Neurosci Lett 402:273–277.

Micheloyannis S, Pachou E, Stam CJ, Breakspear M, Bitsios P, Vourkas M, Erimaki S, Zervakis M (2006b): Small-world networks and disturbed functional connectivity in schizophrenia. Schizophr Res 87:60–66.

Milgram S (1967): The small world problem. Psychol Today 1: 61–67.

Montez T, Linkenkaer-Hansen K, van Dijk BW, Stam CJ (2006): Synchronization likelihood with explicit time-frequency priors. Neuroimage 33:1117–1125.

Neale MC, Boker SM, Xie G, Maes HH (2003): Mx: Statistical Modeling, 6th ed. http://www.vcu.edu.mx

Newman ME. (2003): The structure and function of complex networks. SIAM Rev 45:167.

Pereda E, Quiroga RQ, Bhattacharya J (2005): Nonlinear multivariate analysis of neurophysiological signals. Prog Neurobiol 77:1–37.

Ponten SC, Bartolomei F, Stam CJ (2007): Small-world networks and epilepsy: Graph theoretical analysis of intracerebrally recorded mesial temporal lobe seizures. Clin Neurophysiol 118:918–927.

Posthuma D, Neale MC, Boomsma DI, de Geus EJ (2001): Are smarter brains running faster? Heritability of alpha peak frequency, IQ, and their interrelation. Behav Genet 31:567–579.

Posthuma D, Beem AL, de Geus EJ, Van Baal GC, von Hjelmborg JB, Iachine I, Boomsma DI (2003): Theory and practice in quantitative genetics. Twin Res 6:361–376.

Posthuma D, de Geus EJ, Mulder EJ, Smit DJ, Boomsma DI, Stam CJ (2005): Genetic components of functional connectivity in the brain: the heritability of synchronization likelihood. Hum Brain Mapp 26:191–198.

Rulkov NF, Sushchik MM, Tsimring LS, Abarbanel HD (1995): Generalized synchronization of chaos in directionally coupled chaotic systems. Phys Rev E 51:980–994.

Smit DJ, Posthuma D, Boomsma DI, Geus EJ (2005): Heritability of background EEG across the power spectrum. Psychophysiology 42:691–697.

Stam CJ (2004): Functional connectivity patterns of human magnetoencephalographic recordings: A "small-world" network? Neurosci Lett 355:25–28.

Stam CJ (2005): Nonlinear dynamical analysis of EEG and MEG: Review of an emerging field. Clin Neurophysiol 116:2266–2301.

Stam CJ (2006): Nonlinear Brain Dynamics. New York: Nova Science.

Stam CJ, van Dijk BW (2002): Synchronization likelihood: An unbiased measure of generalized synchronization in multivariate data sets. Psysica D 163:236–251.

Stam CJ, Breakspear M, van Cappellen van Walsum AM, van Dijk BW (2003): Nonlinear synchronization in EEG and whole-head MEG recordings of healthy subjects. Hum Brain Mapp 19:63–78.

Stam CJ, Nolte G, Daffertshofer A. Phase lag index: Assessment of functional connectivity from multi channel EEG and MEG with diminished bias from common sources. Hum Brain Mapp. (in press).

Theiler J (1986): Spurious dimension from correlation algorithms applied to limited time-series data. Phys Rev A 34:2427–2432.

Watts DJ, Strogatz SH (1998): Collective dynamics of "small-world" networks. Nature 393:440–442.